Luminescent ruthenium(II) complexes used for the detection of 8oxoguanine in the human telomeric sequence

Martin Gillard, Hugues Bonnet, Rémy Lartia, Hiba Yacoub, Jérôme Dejeu, Eric Defrancq, Benjamin Elias

Luminescent ruthenium(II) complexes used for the detection of 8-oxoguanine in the human telomeric sequence

Journal:	*Bioconjugate Chemistry*
Manuscript ID	bc-2022-00578u.R1
Manuscript Type:	Article
Date Submitted by the Author:	08-Jan-2023
Complete List of Authors:	Gillard, Martin; Université catholique de Louvain, Chemistry Bonnet, Hugues; Université Grenoble Alpes Lartia, Remy; Communaute d'Universites et Etablissements Universite Grenoble Alpes, Dpt of Molecular chemistry Yacoub, Hiba; Université Grenoble Alpes Dejeu, Jerome; Departement de Chimie Moleculaire, Biomolecular Engineering and Interadction Defrancq, Eric; Universite Grenoble Alpes, Departement de chimie moléculaire Elias, Benjamin; Universite catholique de Louvain, Institute of Condensed Matter and Nanosciences

Luminescent ruthenium(II) complexes used for the detection of 8-oxoguanine in the human telomeric sequence

Martin Gillard, † Hugues Bonnet, ‡ Rémy Lartia, ‡ Hiba Yacoub, ‡ Jérôme Dejeu, ‡,§ Eric Defrancq*‡ and Benjamin Elias*†

† Université catholique de Louvain (UCLouvain), Institut de la Matière Condensée et des Nanosciences (IMCN), Molecular Chemistry, Materials and Catalysis (MOST), Place Louis Pasteur 1, bte L4.01.02, B-1348 Louvain-la-Neuve, Belgium

‡ Université Grenoble-Alpes (UGA), Département de Chimie Moléculaire, UMR CNRS 5250, CS 40700, 38058 Grenoble, France

§ FEMTO-ST Institute, CNRS UMR-6174, Université de Bourgogne Franche-Comté, F-25000 Besançon, France

ABSTRACT: Detecting cancer at the early stage of the disease is crucial to keep the best chance for successful treatment. The recent development of genomic screening, a methodology that is addressed to asymptomatic patients presumably at risk of carcinogenesis, has stimulated the quest for new tools able to signal the level of risk. Carcinogenesis has been associated to chronic oxidative stress exceeding the antioxidant defenses and leading to critical genome alteration levels. The telomeric regions are presumably the most exposed to oxidative stress due to their high concentration of guanine (*i.e.* the easiest oxidizable nucleic base). Accumulation of 8-oxoguanine in telomeres, thus oxidative lesions, was reportedly associated with telomeric crisis and carcinogenesis. In this study, we report on the capacity of Ru(II) polyazaaromatic complexes to photoprobe 8-oxoguanine into the human telomeric sequence with the view of developing new tools for cancer risk screening.

Introduction

Diagnosis of cancer currently focuses on detecting early carcinogenesis stage in patients to give them the best chance for successful treatment.[1] Unfortunately, in the case of aggressive tumours, the cancer has already reached an advanced stage when the first symptoms are detected. This has stimulated the development of screening methods based on different strategies than early diagnosis. Screening is more specifically addressed to apparently healthy and asymptomatic patients that are presumably having a high risk of carcinogenesis.[2] Efficient screening requires the development of new tests or examinations that can be used rapidly and easily. In this context, the detection of cellular oxidative stress signals is of major interest. [3] Indeed, chronic acute oxidative stress is a great contributor to the development of numerous diseases including cancer. It consists in the presence of a too high level of reactive oxygen species (ROS) exceeding the antioxidant defences of the organism. This can be attributed to diverse environmental and intrinsic factors.[4-7] Excess of ROS can cause irreversible oxidative damages to DNA, which is particularly critical at the level of telomeres as they play a pivotal role for genome stability and integrity. Studies in mouse models, human tissues and cell culture provided evidence that oxidative stress promote and accelerate telomere dysfunction.[8-10] The loss of telomeres maintenance was reported to contribute to ageing-related diseases, telomere crisis and carcinogenesis.[11, 12] This can be explained by the high sensitivity of telomeres to ROS resulting from their high concentration in guanine, the easiest oxidizable nucleic base ($E_{G^{\cdot}/G}$ = + 1.29 V *vs* NHE).[13] The guanine oxidation mainly leads to the formation of 8-oxoguanine (8-oxoG), the most studied DNA damage by far, which once persistent in telomeres promotes the above mentioned telomere loss and crisis.[14] The detection of telomeric 8-oxoG may lead to the development of new screening tools able to sense a risk of carcinogenesis at the earliest stage.[15-18]

The human telomeric DNA sequence (hTel) varies from 2-50 kilobases of approximately 300-8,000 repeats of the sequence (-TTAGGG-). As a result of their high concentration in guanines, telomeres can adopt a quadruple helix structure, namely G-quadruplex (G4) consisting in the assembly of four guanines forming a guanine quartet through Hoogsteen bonds.[19, 20] Studies reporting on the impact of oxidative lesions on the human telomeric G4 DNA structure stability were recently reported.[21-23] The destabilizing effect on the G4 structure due to reduced hydrogen-bonding ability caused by the replacement of a guanine residue by 8-oxoG was evaluated. It appeared that the 8-oxoG position into the G4 structure has a major impact on its stability.[24]

During the last decades, many studies demonstrated the abilities of ruthenium (II) complexes as "DNA light switch" or as DNA specific sites photoprobes *in vitro* or *in cellulo*.[25-37] In the present study, we aim at investigating the potential of Ru(II) polyazaaromatic complexes as 8-oxoG photoprobes in telomeric DNA and in duplex DNA. Complexes $[Ru(bpy)_2napp]^{2+}$ **1**, $[Ru(phen)_2cpip]^{2+}$ **2** and $[Ru(phen)_2salphen]^{2+}$ **3** (**Figure 1**) that are present as a mixture of *Λ* and Δ isomers were chosen for their reported ability to discriminate DNA topologies (such as G4 DNA and DNA mismatches) thanks to their high luminescence sensitivity.[38-40] We report on a brief description of the synthesis and the photophysical properties of compounds **1-3** along with a more detailed study of their 8-oxoG photoprobing capacities. This was achieved thanks to luminescence titrations using five different oligodeoxynucleotides (ODN's) that incorporate (or not) an 8-oxoG residue. Three selected ODN's **hTel**, **hTel-oxoG21** and **hTel-oxoG10** are based on the human telomeric sequence. They fold into G4 architectures as reported by Podbevšek and co-workers,[24] with **hTel-oxoG21** and **hTel-oxoG10** including an 8-oxoG at the outer or at the central quartet of the G4, respectively (**Figure 2**). The two others selected ODN's **HP** and **HP-oxoG** are G-rich sequences that fold into a duplex hairpin shape with **HP-oxoG** including an oxo-G residue in the middle of the helix (see the structures in the supporting information).

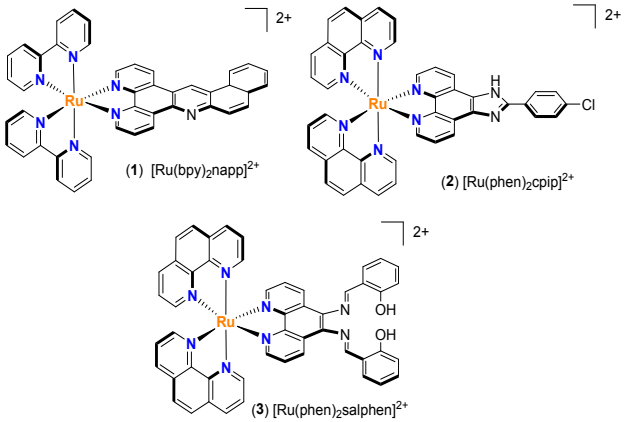

Figure 1. Structures of $[Ru(bpy)_2napp]^{2+}$ **1**, $[Ru(phen)_2cpip]^{2+}$ **2** and $[Ru(phen)_2salphen]^{2+}$ **3**.

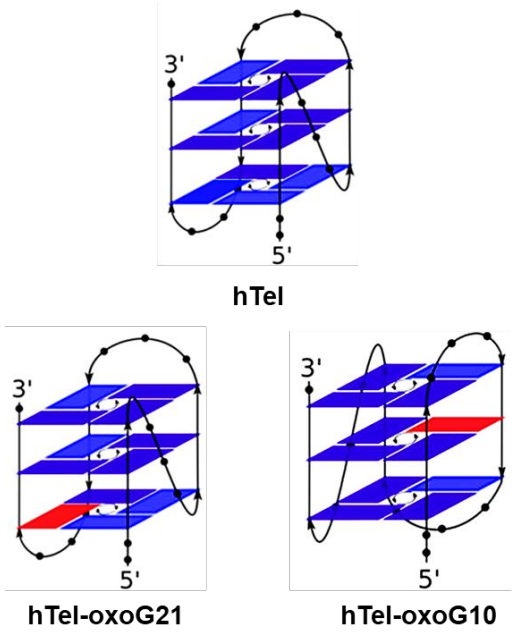

Figure 2. Schematic representation of the **hTel**, **hTel-oxoG21** and **hTel-oxoG10** oligonucleotides used in this study. The sequences are: **hTel** ($^{3'}$A(GGGATT)$_3$GGGTT$^{5'}$), **hTel-oxoG21** ($^{3'}$A GG^{oxo}G/ATT(GGGATT)$_2$GGGTT$^{5'}$), **hTel-oxoG10** ($^{3'}$A(GGGATT)$_2$G^{oxo}G/GATTGGGTT$^{5'}$).

Results and Discussion

Synthesis

Complexes **1-3** were prepared by the chelation of napp, cpip or salphen ligands onto $[Ru(bpy)_2Cl_2]$ or $[Ru(phen)_2Cl_2]$ using previously published methods.[38-40] Complexes **1-3** were isolated as orange powders after purification on silica and were characterized by ^{1}H-NMR spectroscopy and HRMS. Compound **1** was also characterised by X-ray crystallography.[40] The $[Ru(bpy)_3]^{2+}$ and $[Ru(phen)_3]^{2+}$ references were synthesized and purified according to reported synthetic routes from the hydrated $RuCl_3$ salt (see the synthesis and characterization of the complexes in the supporting information).

Electrochemistry

In terms of electrochemical properties, compounds **1-3** display oxidation potentials that are very close to those of the reference compounds $[Ru(bpy)_3]^{2+}$ and $[Ru(phen)_3]^{2+}$ (1.34 V and 1.32V *vs* Ag/AgCl). This corresponds to the Ru^{2+}/Ru^{3+} oxidation, which suggests that the HOMO of the compounds is metal centred (**Table 1**). Conversely, the potentials of first oxidation appear to be very different ranging from -0.77 V for complex **2** to -1.24 V for complex **1**. The strong influence of the extended ligand structure on the potential of first reduction of compounds **1-3** indicates that their LUMO orbitals lay on their extended ligands. It appears that the cpip ligand in complex **2** is responsible for a strong stabilization of the LUMO orbital compared to napp and salphen ligands in compounds **1** and **3**, which can be attributed to the strong electron stabilizing effect induced by the conjugated imidazole moiety. The next two reduction waves of compounds **1-3** all occur at very similar potentials to those of the reference complexes $[Ru(bpy)_3]^{2+}$ and $[Ru(phen)_3]^{2+}$ and correspond to the subsequent reductions of each bipyridine/phenanthroline ancillary ligands (-1.47 V and -1.71 V *vs* Ag/AgCl, for $[Ru(bpy)_3]^{2+}$).

Table 1. Oxidation ($E_{1/2\ ox}$) and reduction ($E_{1/2\ red}$) potentials of complexes **1-3** and reference complexes.

Complex	$E_{1/2ox}$[a][V][b]	$E_{1/2\ red}$ [a] [V][b]		
$[Ru(bpy)_3]^{2+}$	+ 1.34	-1.28	-1.47	-1.71
$[Ru(phen)_3]^{2+}$	+ 1.32	-1.30	-1.47	-1.68
$[Ru(bpy)_2napp]^{2+}$ **1**	+ 1.35	-1.24	-1.38	-1.65
$[Ru(phen)_2cpip]^{2+}$ **2**	+ 1.37	-0.77	- 1.43	-1.63
$[Ru(phen)_2salphen]^{2+}$ **3**	+1.36	-0.91	-1.45	-1.64

[a] Measured in dry acetonitrile. The electrochemical data for complexes $[Ru(bpy)_3]^{2+}$ and $[Ru(phen)_3]^{2+}$ are from references.[32, 41, 42]

Light absorption

The light absorption data of compounds **1-3** were measured at room temperature in acetonitrile (**Figure 3** and **Table 2**). The recorded spectra are typical of polyazaaromatic Ru(II) complexes and are very close to the one of $[Ru(bpy)_3]^{2+}$.[41] Analysis of the data obtained for **1-3** allows to ascribe the UV absorption bands ($\varepsilon \approx 10^5$ $M^{-1}cm^{-1}$) to ligand centred transitions. Particularly, the band arising at *ca.* 285 nm in compound **1** and $[Ru(bpy)_3]^{2+}$ is attributed to the absorption of the bpy ligands while the band at *ca.* 265 nm in compounds **2** and **3** and in $[Ru(phen)_3]^{2+}$ is attributed to the phen ligands. The observed strong absorption bands in the visible region at *ca.* 450 nm ($\varepsilon \approx 10^4$ $M^{-1}cm^{-1}$) arise from metal-to-ligand charge-transfer (MLCT). Complex **1** displays the strongest visible light absorptivity (ε = 2.48 x 10^4 $M^{-1}cm^{-1}$ at 456 nm) among the reported compounds.

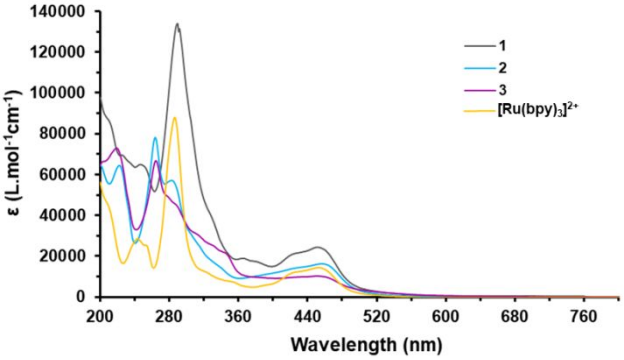

Figure 3. Absorption spectra of complexes **1-3** and $[Ru(bpy)_3]^{2+}$ in acetonitrile under air.

Table 2. Light absorption bands and absorption coefficients in acetonitrile for complexes **1-3** and references.

Complex	Absorption λ_{max}[nm] (ε [10^4 L.mol^{-1}.cm^{-1}])[a]
$[Ru(bpy)_3]^{2+}$	250, 285 (8.71), 345 (sh), 452 (1.45)
$[Ru(phen)_3]^{2+}$	265, 287 (sh), 418 (sh), 447 (1.84)
$[Ru(bpy)_2napp]^{2+}$ **1**	246, 289 (13.6), 343 (sh), 456 (2.48)
$[Ru(phen)_2cpip]^{2+}$ **2**	265, 287 (sh), 335 (sh), 460 (1.61)
$[Ru(phen)_2salphen]^{2+}$ **3**	265, 288 (sh), 338 (sh), 458 (1.04)

[a] Measurements were carried out at room temperature. sh = shouldering peaks. The absorption data for $[Ru(bpy)_3]^{2+}$ are from references.[32, 41, 42]

Table 3. Emission data in CH_3CN and H_2O at 298 K for complexes **1-3** and reference complexes.

Complex	Emission λ_{max} [a,b] [nm]		Φ_{em} [c,d]		τ_{em} [ns] [c]		k_r [10^3 s^{-1}]	
	CH_3CN	H_2O	CH_3CN	H_2O	CH_3CN	H_2O	CH_3CN	H_2O
$[Ru(bpy)_3]^{2+}$	604	604	0.094	0.063	855	630	77	69
$[Ru(phen)_3]^{2+}$	604	606	0.028	0.072	460	920	61	75
$[Ru(bpy)_2napp]^{2+}$ **1**	601	606	0.072	0.12	812	841	89	143
$[Ru(phen)_2cpip]^{2+}$ **2**	597	603	0.058	0.14	380	1315	152	106
$[Ru(phen)_2salphen]^{2+}$ **3**	599	600	0.018	0.075	688	1222	26	61

Measurements were done on air equilibrated solutions. [b] λ_{exc} = 450 nm. [c] Measurements made with a 5 µmol L^{-1} concentration in complex under argon. [d] Measurements relative to $[Ru(bpy)_3]^{2+}$ in argon purged solution (Φ_{em} = 0.063) or in nitrogen purged acetonitrile (Φ_{em} = 0.094).[43] The photophysical data for $[Ru(bpy)_3]^{2+}$ and $[Ru(phen)_3]^{2+}$ are from reference.[20]

Light emission

The light emission properties of complexes **1-3** including their luminescence wavelengths, quantum yields, and lifetimes were recorded in water and in acetonitrile and are gathered in **Table 3** along with those of $[Ru(bpy)_3]^{2+}$ and $[Ru(phen)_3]^{2+}$. Complexes **1-3** exhibit luminescence properties that are very close to those of the reference complexes $[Ru(bpy)_3]^{2+}$ and $[Ru(phen)_3]^{2+}$ with a broad unstructured emission at about 600 nm. The emission is also strongly dependent on the solvent polarity and relatively long (≈ microsecond) lifetimes of the excited states typical of ^{3}MLCT-emissive transition were measured. In addition, the bathochromic shift of the compounds' luminescence on going from acetonitrile to the more polar water and their large k_r values (> 10^4 s^{-1}) confirm the charge-separated excited states as reported for $[Ru(bpy)_3]^{2+}$ and $[Ru(phen)_3]^{2+}$.

Luminescence titrations

As mentioned in the introduction, ruthenium (II) complexes **1-3** were mainly selected for their reported abilities to photoprobe specific DNA topologies. While compound **1** has been previously reported to photodetect DNA mismatches, compounds **2** and **3** have been shown to act as G4 DNA photoprobes. This originates from the combination of (i) the high sensitivity of the polyazaaromatic Ru(II) complexes luminescence to the microenvironment with (ii) an appropriate structural design of the napp, cpip and salphen interacting ligands. In the present work, the ability of compounds **1-3** to photoprobe 8-oxoG lesions in G-quadruplex and in duplex DNA was assessed using five short ODN's. The **hTel-oxoG21** and **hTel-oxoG10** sequences were recently exploited by Podbevšek and co-workers and allowed to highlight the major impact of the 8-oxoG lesion localization on the conformation and stability of the resulting G4 structures. [24]

They showed that the **hTel-oxoG10** G4 containing the 8-oxoG in the central G-quartet leads to structural rearrangement while the **hTel-oxoG21** G4 containing the 8-oxoG in the outer G-quartet retains the parent G4 fold. This may lead to differences in terms of interaction and luminescence properties in the presence of photoprobes **1-3**. The steady state luminescence titration curves of compound **1** in the presence of the five DNA models are displayed in **Figure 4A** and **4B** (see the supporting information for compounds **2** and **3**). The great increases of luminescence intensity in the presence of **hTel**, **hTel-oxoG21** and **hTel-oxoG10** are reported in **Figure 5A** and allow to assess the photoprobing ability of compounds **1-3** for the different G4 folding sequences. As displayed in **Figure 5B**, complexes **1-3** show very close increases of luminescence intensity in

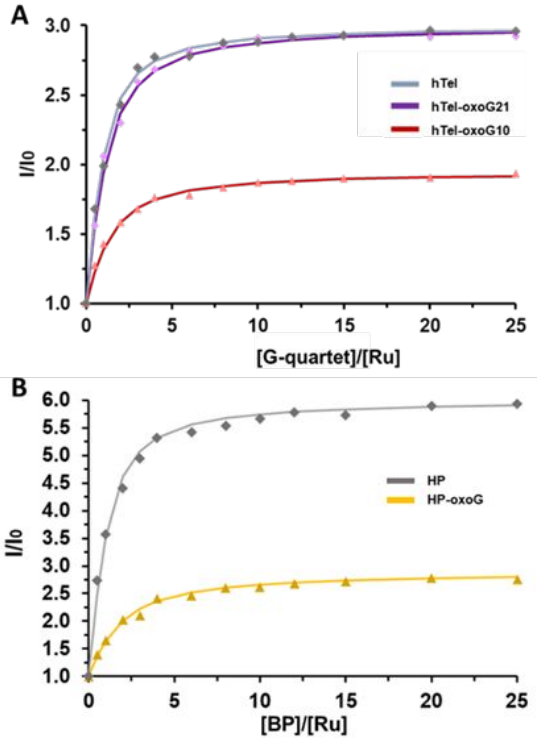

Figure 4. Relative luminescence intensity (I/I_0) of complex **1** as a function of the relative (**A**) G-quartet or (**B**) base pair concentration. I_0 is the luminescence of the complex without DNA. Measurements were carried out in solutions of 2.5 µM of complex in 10 mM HEPES buffer, with 100 mM NaCl and 50 mM KCl at pH 7.4. Excitation at 450 nm. The McGhee–von Hippel equation was implemented to fit the curves.

the presence of **hTel** and **hTel-oxoG21**, with complex **3** showing the strongest luminescence increase when interacting with G4 DNA (+224 and +247% in the presence of **hTel** and **hTel-oxoG21**, respectively). Conversely, the increase of luminescence intensity of complexes **1-3** appeared to be drastically reduced in the presence of the central 8-oxoG containing G4 structure **hTel-oxoG10**. Complex **2** revealed to be the best candidate to discriminate the central 8-oxoG containing G4 from the two other sequences (+72% *vs* +152-166%). A similar behaviour was observed for the duplex hairpin ODN's, as the increases of luminescence intensities of the three complexes **1-3** revealed to be significantly attenuated in the presence of the **HP-oxoG** against **HP**. Complex **1** revealed to be the most discriminant compound showing a fall of the luminescence increase from +494% *vs* **HP** to a weaker +177% *vs* **HP-oxoG**.

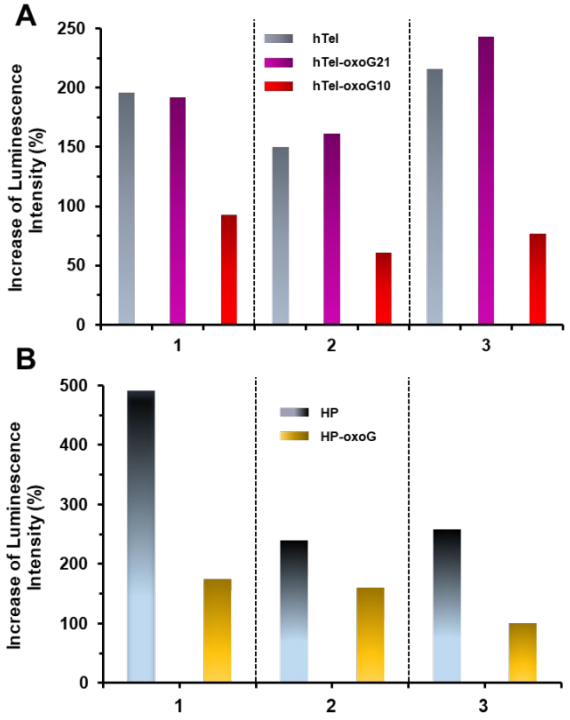

Figure 5. Increase of luminescence intensities (in %) for complexes **1-3** in the presence of (**A**) **hTel**, **hTel-oxoG21** and **hTel-oxoG10** and (**B**) **HP** and **HP-oxoG**. The results are reported as increase percentage compared to the luminescence of the compound without DNA. Measurements were done on 2.5 µM solutions of complex in 10 mM HEPES buffer, with 100 mM NaCl and 50 mM KCl at pH 7.4.

The dissociation equilibrium constants (K_D) values of the interaction between complexes **1-3** for the five DNA models were estimated using a modified McGhee-von Hippel model that fits the titration curves (**Table 4**).[44] The K_D values of the interaction of the compounds with the G4 DNA models **hTel, hTel-oxoG21** and **hTel-oxoG10** appear to be in the tenth of micromolar range. Each of the three complexes displays very close K_D values for the different studied sequences, ranging from 11 µM for compound **1** *vs* **hTel** to 43 µM for compound **3** *vs* **hTel-oxoG10**. The three compounds also display the same trend in terms of affinity for the three sequences with the affinity decreasing in this order: **hTel; hTel-oxoG21; hTel-oxoG10** (complex **1**: 11; 19; 22 µM, complex **2**: 14; 17; 31 µM and complex **3** 23, 28, 43 µM). The K_D values of the interaction of the complexes with the duplex DNA models **HP** and **HP-oxoG** are in the micromolar range for compound **1** and is one to two orders of magnitude higher for compounds **2** and **3** as previously reported. Complex **1** appears to be more affine for **HP** *vs* **HP-oxoG** (12 *vs* 47 µM) while compounds **2** (205 *vs* 62 µM) and **3** (176 *vs* 44 µM) are more affine for the 8-oxoG containing hairpin. The luminescence titration data demonstrate the very low impact of the presence of the 8-oxoG lesion on the interaction strength both for G4 and duplex HP type DNA. They also highlight the high sensitivity of the compounds to their local environment, especially when interacting with DNA. The ability of compounds **1-3** to photoprobe 8-oxo-G containing ODN's in **hTel-oxoG10** and **HP-oxoG** over their parent ODN's **hTel** and **HP** presumably arises from a poorer protection of the excited complexes in the 8-oxo-G containing ODN's towards non-radiative

Table 4. Dissociation equilibrium constants (K_D) estimated for **1-3** with the five DNA models.

ODN	Constants	1	2	3
hTel	I/I_0 max	3.0	2.5	3.2
	K_D (µM)	11	14	23
hTel-oxoG21	I/I_0 max	2.9	2.6	3.4
	K_D (µM)	19	17	28
hTel-oxoG10	I/I_0 max	1.95	1.6	1.7
	K_D (µM)	22	31	43
HP	I/I_0 max	5.9	3.4	3.5
	K_D (µM)	17	247	192
HP-oxoG	I/I_0 max	2.7	2.6	2.0
	K_D (µM)	52	72	55

A McGhee-von Hippel type equation was used to assess the K_D values; the binding site was fixed to three base pairs or to one G4 per complex (best fit). Errors are estimated to 5%.

Bio-Layer interferometry studies

Bio-layer interferometry analysis (BLI) was performed to further determine the parameters of the interaction of compounds **1-3** with the five ODN's. The association and dissociation constants between the complexes and the targets were measured, which give access to the dissociation equilibrium constant (K_D). BLI was first implemented to study interactions between large biomolecules, such as protein–membrane interactions and more recently for the interaction of small compounds with G4 DNA.[38, 45, 46] The studies were done in the same saline conditions than luminescence titrations (10 mM HEPES pH 7.4, 100 mM NaCl, 50 mM KCl). BLI sensorgrams recorded for the interaction of complex **1** with the **hTel** and **hTel-oxoG10** are displayed in **Figure 6A** and in **Figure 6B**, respectively (see the supporting information for the other sensorgrams). As revealed by the fitting of the luminescence titration curves, compounds **1-3** exhibit K_D values in the tenth of micromolar range for their interaction with the different G4

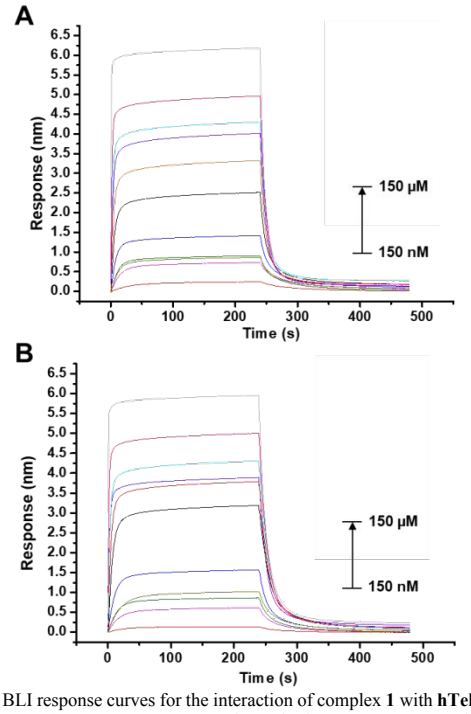

Figure 6. BLI response curves for the interaction of complex **1** with **hTel** (A) and **hTel-oxoG10** (B). Measurements are performed using 0.15 to 150 µM of complex in 10 mM HEPES pH 7.4, 100 mM NaCl, 50 mM KCl.

Table 5. BLI analysis data for the interactions of complexes **1-3** with the studied ODN's.

ODN	Constant	1	2	3
hTel	k_{on} (10^3 M^{-1} s^{-1})	2.4 ± 0.7	1.1 ± 0.3	3.6 ± 1.1
	k_{off} (s^{-1})	50 ± 10	40 ± 20	47 ± 15
	K_D (μM)	19 ± 3	10 ± 5	15 ± 8
hTel-oxoG21	k_{on} (10^3 M^{-1} s^{-1})	2.9 ± 1.2	1.1 ± 0.2	4.4 ± 1.3
	k_{off} (s^{-1})	70 ± 20	6 ± 3	64 ± 20
	K_D (μM)	34 ± 8	7 ± 3	24 ± 11
hTel-oxoG10	k_{on} (10^3 M^{-1} s^{-1})	2.5 ± 0.9	0.8 ± 0.2	2.8 ± 1.2
	k_{off} (s^{-1})	80 ± 20	6 ± 2	78 ± 12
	K_D (μM)	33 ± 7	7 ± 2	35 ± 16
HP	k_{on} (10^3 M^{-1} s^{-1})	1.3 ± 0.3	n.d.[a]	2.0 ± 0.9
	k_{off} (s^{-1})	90 ± 10	n.d.[a]	100 ± 30
	K_D (μM)	82 ± 28	n.d.[a]	76 ± 16
HP-oxoG	k_{on} (10^3 M^{-1} s^{-1})	2.7 ± 0.9	n.d.[a]	1.4 ± 0.4
	k_{off} (s^{-1})	110 ± 40	n.d.[a]	148 ± 4
	K_D (μM)	73 ± 29	n.d.[a]	116 ± 34

Equilibrium dissociation constants were deduced from the kinetic rate constants. [a] The weak binding of the complex the oligonucleotides did not allow to determine the kinetic parameters of the interactions (n.d.) in the studied concentration range. Running buffer: 10 mM HEPES pH 7.4, 100 mM NaCl, 50 mM KCl. Measurements are performed using 0.15 to 150 μM of complex in 10 mM HEPES pH 7.4, 100 mM NaCl, 50 mM KCl.

folding ODN's **hTel**, **hTel-oxoG21** and **hTel-oxoG10** (**Table 5**).

Conclusions

A series of three Ru(II) polyazaaromatic complexes were prepared. The compounds were selected as they were reported for their ability to photoprobe DNA specific sites thanks to their highly sensitive luminescence properties. A series of five ODN's that contain (or not) an 8-oxoG moiety were chosen and tested. This includes three G4 folding oligomers based on the human telomeric sequence, namely **hTel, hTel-oxoG21** and **hTel-oxoG10** and two duplex hairpin folding oligomers, namely **HP** and **HP-oxoG**. Steady state luminescence titrations revealed the ability of the three compounds to discriminate the **hTel-oxoG10** sequence that imbedded an 8-oxoG lesion into the G4's central quartet over the sequences **hTel** and **hTel-oxoG21** with respective luminescence increase of +72% *vs* +224-247% for the most discriminating complex. A similar trend was observed for the duplex hairpin **HP** that gave higher luminescence increases than for **HP-oxoG** (+494% *vs* **HP** to a weaker +177% *vs* **HP-oxoG**). The ability of the compounds **1-3** to photoprobe 8-oxo-G containing ODN's in **hTel-oxoG10** and **HP-oxoG** over their parent ODN's presumably arises from their lower ability to protect the compounds against non-radiative deexcitation sources (e.g. solvent collisions and oxygen sensitization). This probably results from the lower stability and consequent looser structure of **hTel-oxoG10** and **HP-oxoG**. Fitting of the luminescence titrations curves using a modified McGhee–von Hippel equation associated with results obtained from bio-layer interferometry studies allowed to make an in-depth study of the interaction between the complexes and the five ODN's. The results obtained showed that the compounds interact with the different ODN's within the tenth micromolar range for K_D values. They also highlighted that the presence of 8-oxoG had non-significant impact on the parameters of the interaction (k_{on}, k_{off} or K_D) of the complexes with both duplex hairpin and G4 folding sequences. Altogether, the results from luminescence titrations presented herein show promises for the development of sensitive photoprobes for the rapid detection and quantification of 8-oxoG in human telomeric DNA.

Experimental section

Materials and instrumentation

$[Ru(bpy)_2Cl_2]$ and $[Ru(phen)_2Cl_2]$ precursors, napp, cpip and salphen ligands were prepared based on methods reported in the literature. [38-40] Reagents and solvents used for synthesis were of reagent grade and were used without any further purification. The solvents for electrochemical and spectroscopic studies were of spectroscopic grade. Water was purified with a Millipore Milli-Q system. Hairpin ODNs 29-mer **HP** ($^{3'}$CCGT(C)$_3$TACCG(T)$_5$CGGTA(G)$_3$ACGG$^{5'}$) and **HP-oxoG** ($^{3'}$CCGT(C)$_3$TACCG(T)$_5$CGGTA/^{oxo}G/GGACGG$^{5'}$) were purchased from Eurogentec. G4 ODNs 24-mer **hTel** ($^{3'}$A(GGGATT)$_3$GGGTT$^{5'}$), **hTel-oxoG21** ($^{3'}$AGG/^{oxo}G/ATT(GGGATT)$_2$GGGTT$^{5'}$), **hTel-oxoG10** ($^{3'}$A(GGGATT)$_2$G/^{oxo}G/GATTGGGTT$^{5'}$) were synthesied by standard automated solid phase ODN synthesis on a 3400 DNA synthesizer. After purification by RP-HPLC, they were thoroughly desalted by size-exclusion chromatography (SEC). DNA and ODN concentrations were determined spectroscopically. Biotinylated ODN's were prepared on a Controlled Pore Glass solid support by using the phosphoramidite approach with an Applied Biosystems 3400 DNA/RNA Synthesizer (1 μmol scale). Before each experiment the oligonucleotides were annealed by heating at 90 °C for 5 minutes prior to a slow cooling to room temperature over one hour to ensure their folding into G-quadruplex or hairpin duplex structure. NMR experiments were done in d^6-DMSO, CD_3OD or CD_3CN on a Bruker AC-300 Avance II (300 MHz) or on a Bruker AM-500 (500 MHz) at 20 °C. The NMR shifts were measured *vs* the residual peak of the solvent as the internal standard. High-resolution mass spectrometry (HRMS) spectra were recorded on a Q-Exactive orbitrap from ThermoFisher using reserpine as the internal standard. Samples were ionized by electrospray ionization (ESI; capillary temperature = 320 °C, vaporizer temperature = 320 °C, sheath gas flow rate = 5 mL min^{-1}).

Cyclic voltammetry was performed using a platinum wire counter electrode, a glassy carbon disk working electrode with an area of *ca.* 0.03 cm^2 and a reference electrode of Ag/AgCl. The working electrode potential was monitored thanks to an Autolab PGSTAT 100 potentiostat and *via* a computer interface. The cyclic voltammograms were measured in dried acetonitrile using a sweep rate of 300 mV s^{-1}. The complex's concentration was 0.8 mmol L^{-1}, and tetrabutylammonium hexafluorophosphate was used as the supporting electrolyte (C =0.1 mol L^{-1}). The samples were purged by nitrogen before each use.

Light absorption data were recorded on a Shimadzu UV-1700 spectrophotometer. Luminescence data were recorded on a Varian Cary Eclipse instrument. Quantum yields were obtained using $[Ru(bpy)_3]^{2+}$ as a reference.[43] The luminescence lifetime measurements were performed at the second harmonic of a titanium crystal at λ=450 nm with a sapphire laser (picosecond Tsunami laser Spectra at a repetition rate of 80 kHz). A Fluotime 200 instrument from AMS Technologies was used for the decay acquisition. It consists of a GaAs microchannel plate photomultiplier tube (Hamamatsu model R3809U-50) followed by a time-correlated single-photon counting system from Picoquant (PicoHarp300). Luminescence decays were analyzed with FLUOFIT software. The time resolution of the system is of *ca.*4 ps. Luminescence titrations were done in the following buffer: 10 mM HEPES pH 7.4, 50 mM NaCl and 100 mM KCl. The complex concentration was kept at 5 μM.

Bio-layer interferometry experiments were performed using sensors coated with streptavidin (SA sensors) purchased from Forte Bio (SARTORIUS). Prior to use, they were immersed for 10 minutes in a buffer before functionalization to dissolve the sucrose layer. Then the sensors were dipped for 15 minutes in DNA containing solutions (biotinylated hairpin ODN's) at 100

nM and rinsed in the buffer solution (10 mM HEPES, 50 mM NaCl, 100 mM KCl (pH 7.4), 0.5% v/v surfactant P20) for 10 minutes. The functionalized sensors were next dipped in the ruthenium complex containing solution at different concentrations (see supporting information) for 4 minutes interspersed by a rinsing step in the buffer solution for 4 minutes. Reference sensors without DNA immobilization were used to subtract the non-specific adsorption on the SA layer. The sensorgrams were fit using a 1:1 interaction model. The reported values are the means of representative independent experiments, and the errors provided are standard deviations from the mean. Each experiment was repeated at least two times using a concentration range from 0.5 µM to 150 µM.

Synthetic procedures and characterization

$[Ru(bpy)_2napp]^{2+}$ 1. $[Ru(bpy)_2Cl_2]$ (20 mg, 0.041 mmol, 1.0 eq.) and the napp ligand (20 mg, 0.061 mmol, 1.5 eq) were dissolved in an EtOH/H_2O mixture (5/5 - v/v, 5 mL). The reaction medium was heated at 80 °C under stirring to the entire consumption of the ligand while monitored by TLC (3 h). EtOH was then removed under *vacuum* and NH_4PF_6 was added yielding precipitation of the complex. The so-formed orange solid was washed with water, EtOH and dried *in vacuo*. The crude product was finally purified by chromatography on silica (10:1:0.5 $CH_3CN/H_2O/$ KNO_{3sat}) which gave $[Ru(bpy)_2napp]^{2+}$ **1** (31 mg, 0.030 mmol, 73%). The exchange from of counter anion from PF_6^- to Cl^- was done by the addition of NBu_4Cl to an acetone solution of the complex. R_f 0.35 ($CH_3CN/H_2O/$ KNO_{3sat} 10:1:0.5); ^1H NMR (CD_3CN, 500 MHz) δ (ppm), 10.47 (1H, s, H_d), 9.81 (1H, d, $J_{a\text{-}b}$ = 8.2, $J_{a\text{-}c}$ = 1.2 Hz, *Ha*), 9.59 (1H, dd, $J_{c\text{-}b}$ = 8.2, $J_{c\text{-}a}$ = 1.2 Hz, H_c), 9.24 (1H, d, $J_{m\text{-}l}$ = 8.2 Hz, H_m), 8.53 (4H, m, H_5, $H_{5'}$, H_6, $H_{6'}$), 8.34 (1H, d, $J_{i\text{-}j}$ = 9.1 Hz, H_i), 8.25 (1H, d, $J_{j\text{-}i}$ = 9.1 Hz, H_j), 8.16 (2H, m, H_4, $H_{4'}$), 8.12 (3H, m, H_e, H_f, H_g), 8.01 (2H, m, H_7, $H_{7'}$), 7.95 (1H, m, H_l), 7.91-7.84 (5H, m, H_b, H_2, $H_{2'}$, H_m, H_h), 7.73 (1H, d, $J_{9\text{-}8}$ = 5.4 Hz, H_9), 7.69 (1H, d, $J_{9'\text{-}8'}$ = 5.6 Hz, $H_{9'}$), 7.49-7.44 (2H, m, H_3, $H_{3'}$), 7.28-7.21 (m, 2H, H_8, $H_{8'}$); HRMS-ESI calculated for $[C_{43}H_{29}N_7F_6PRu]^+$: *m/z* 890.11728, found: *m/z* 890.11700 and for $[C_{43}H_{29}N_7Ru]^{2+}$: *m/z* 372.57617, found: *m/z* 372.57640.

$[Ru(phen)_2cpip]^{2+}$ 2. The same method used for complex **1** with the precursor $[Ru(phen)_2Cl_2]$ (20 mg, 0.038 mmol) and the cpip ligand (15 mg, 0.045 mmol) gave the crude product that was purified by chromatography on silica ($CH_3CN/H_2O/$ KNO_{3sat} 10:1:0.25) to provide the title compound **2** as an orange powder (30 mg, 0.025 mmol, 68%). R_f 0.30 ($CH_3CN/H_2O/$ KNO_{3sat} 10:1:0.25); ^1H NMR (CD_3CN, 500 MHz) δ 9.05 (d, 1H, J = 8.2 Hz, $H_a/H_{a'}$), 8.89 (d, 1H, J = 8.4 Hz, $H_a/H_{a'}$), 8.59 (dd, 4H, J = 8.3 Hz, J = 1.2 Hz, $H_2/H_{2'}$ *and* $H_9/H_{9'}$), 8.28 (d, 2H, J = 8.7 Hz, H_e *and* $H_{e'}$), 8.25 (s, 4H, H_5 *and* $H_{5'}$; H_6 *and* $H_{6'}$), 8.07 (dd, 2H, J = 10.5 Hz, J = 4.8 Hz, H_8 *and* $H_{8'}$), 8.01 (d, 2H, J = 5.4 Hz, H_7 *and* $H_{7'}$), 7.96 (d, 2H, J = 5.2 Hz, H_4 *and* $H_{4'}$,), 7.67-7.59 (m, 8H, H_3 $H_{3'}$, H_b, $H_{b'}$, H_c, $H_{c'}$, H_d and $H_{d'}$). HRMS Calcd for $[C_{43}H_{27}N_8ClF_6PRu]^+$: *m/z* 931.07595, found: *m/z* 931.07688 Da.

$[Ru(phen)_2salphen]^{2+}$ 3. The same method used for complex **1** with the precursor $[Ru(phen)_2Cl_2]$ (20 mg, 0.038 mmol) and the salphen ligand (16 mg, 0.038 mmol) and gave the crude product that was purified by chromatography on silica ($CH_3CN/H_2O/$ KNO_{3sat} 10:1:0.25) to provide the title compound **3** as an orange powder (33 mg, 0.028 mmol, 75%). R_f 0.31 ($CH_3CN/H_2O/$ KNO_{3sat} 10:1:0.25); ^1H NMR (CD_3CN, 500 MHz) δ 9.03 (broad m, 4H, H_d and H_e), 8.62 – 8.60 (m, 2H, H_2 or H_9), 8.60 – 8.58 (m, 2H, H_2 or H_9), 8.25 (s, 4H, H_5 and H_6), 8.12 – 8.06 (m, 4H, H_7 and H_e), 8.02 (dd, J = 5.2, 1.2 Hz, 2H, H_4), 7.99 (dd, J = 5.3, 1.2 Hz, 2H, H_a), 7.68 (dd, J = 8.3, 5.3 Hz, 2H, H_b), 7.63 (d, J = 5.2 Hz, 2H, H_3 or H_8), 7.61 (d, J = 5.2 Hz, 2H, H_3 or H_8), 7.51 – 7.44 (m, 2H, H_g), 7.17 – 7.06 (m, 4H, H_f and H_h). HRMS-ESI calculated for $[C_{43}H_{28}N_8O^{96}Ru]^{2+}$: *m/z* 384.07255, found: *m/z* 384.07322.

Conflicts of interest

The authors declare no competing interest.

Acknowledgements

M. G. and B. E. gratefully acknowledge the Université catholique de Louvain (UCLouvain) and the F.R.S-FNRS (Grant Number U.N021.21) for financial support. This work was partially supported by the "Agence National de la Recherche", Labex ARCANE (ANR-16-CE11-0006-01), CBH-EUR-GS (ANR-17-EURE-0003), and the région Auvergne-Rhône-Alpes. The NanoBio-ICMG platforms (UAR 2607) are acknowledged for their support.

Supporting Information Available

The supporting information describes the synthesis of the complexes and shows their NMR spectra. Analytical data such as cyclic voltamograms, luminescence titration curves and BLI sensograms are also provided along with a decscription of the models used for the fitting of BLI and luminescence titrations curves.

References

(1) Crosby, D.; Lyons, N.; Greenwood, E.; Harrison, S.; Hiom, S.; Moffat, J.; Quallo, T.; Samuel, E.; Walker, I. A roadmap for the early detection and diagnosis of cancer. *The Lancet Oncology* **2020**, *21* (11), 1397-1399. DOI: https://doi.org/10.1016/S1470-2045(20)30593-3.

(2) Shieh, Y.; Eklund, M.; Sawaya, G. F.; Black, W. C.; Kramer, B. S.; Esserman, L. J. Population-based screening for cancer: hope and hype. *Nature Reviews Clinical Oncology* **2016**, *13* (9), 550-565. DOI: 10.1038/nrclinonc.2016.50.

(3) Katerji, M.; Filippova, M.; Duerksen-Hughes, P. Approaches and Methods to Measure Oxidative Stress in Clinical Samples: Research Applications in the Cancer Field. *Oxid. Med. Cell. Longev.* **2019**, *2019*, 1279250-1279250. DOI: 10.1155/2019/1279250 PubMed.

(4) Møller, P.; Folkmann, J. K.; Forchhammer, L.; Bräuner, E. V.; Danielsen, P. H.; Risom, L.; Loft, S. Air pollution, oxidative damage to DNA, and carcinogenesis. *Cancer Lett.* **2008**, *266* (1), 84-97. DOI: https://doi.org/10.1016/j.canlet.2008.02.030.

(5) Ames, B. N.; Shigenaga, M. K.; Hagen, T. M. Oxidants, antioxidants, and the degenerative diseases of aging. *Proceedings of the National Academy of Sciences* **1993**, *90* (17), 7915-7922. DOI: doi:10.1073/pnas.90.17.7915.

(6) Nakabeppu, Y.; Sakumi, K.; Sakamoto, K.; Tsuchimoto, D.; Tsuzuki, T.; Nakatsu, Y. Mutagenesis and carcinogenesis caused by the oxidation of nucleic acids. **2006**, *387* (4), 373-379. DOI: doi:10.1515/BC.2006.050.

(7) Pizzino, G.; Irrera, N.; Cucinotta, M.; Pallio, G.; Mannino, F.; Arcoraci, V.; Squadrito, F.; Altavilla, D.; Bitto, A. Oxidative Stress: Harms and Benefits for Human Health. *Oxid. Med. Cell. Longev.* **2017**, *2017*, 8416763. DOI: 10.1155/2017/8416763.

(8) Ludlow, A. T.; Spangenburg, E. E.; Chin, E. R.; Cheng, W.-H.; Roth, S. M. Telomeres shorten in response to oxidative stress in mouse skeletal muscle fibers. *The journals of gerontology. Series A, Biological sciences and medical sciences* **2014**, *69* (7), 821-830. DOI: 10.1093/gerona/glt211 PubMed.

(9) Barnes, R. P.; Fouquerel, E.; Opresko, P. L. The impact of oxidative DNA damage and stress on telomere homeostasis. *Mech. Ageing Dev.* **2019**, *177*, 37-45. DOI: https://doi.org/10.1016/j.mad.2018.03.013.

(10) von Zglinicki, T. Oxidative stress shortens telomeres. *Trends Biochem Sci* **2002**, *27* (7), 339-344. DOI: 10.1016/s0968-0004(02)02110-2 From NLM.

(11) Ahmed, W.; Lingner, J. Impact of oxidative stress on telomere biology. *Differentiation* **2018**, *99*, 21-27. DOI: https://doi.org/10.1016/j.diff.2017.12.002.

(12) Dewhurst, S. M. Chromothripsis and telomere crisis: engines of genome instability. *Curr. Opin. Genet. Dev.* **2020**, *60*, 41-47. DOI: https://doi.org/10.1016/j.gde.2020.02.009.

(13) Steenken, S.; Jovanovic, S. V. How Easily Oxidizable Is DNA? One-Electron Reduction Potentials of Adenosine and Guanosine Radicals in Aqueous Solution. *J. Am. Chem. Soc.* **1997**, *119* (3), 617-618. DOI: 10.1021/ja962255b.

(14) Fouquerel, E.; Barnes, R. P.; Uttam, S.; Watkins, S. C.; Bruchez, M. P.; Opresko, P. L. Targeted and Persistent 8-Oxoguanine Base Damage at Telomeres Promotes Telomere Loss and Crisis. *Mol. Cell* **2019**, *75* (1), 117-130.e116. DOI: https://doi.org/10.1016/j.molcel.2019.04.024.

(15) Nakabeppu, Y. Cellular Levels of 8-Oxoguanine in either DNA or the Nucleotide Pool Play Pivotal Roles in Carcinogenesis and Survival of Cancer Cells. *Int. J. Mol. Sci.* **2014**, *15* (7), 12543-12557.

(16) Manavalan, S.; Rajaji, U.; Chen, S.-M.; Steplin Paul Selvin, S.; Govindasamy, M.; Chen, T.-W.; Ajmal Ali, M.; Al-Hemaid, F. M. A.; Elshikh, M. S. Determination of 8-hydroxy-2′-deoxyguanosine oxidative

stress biomarker using dysprosium oxide nanoparticles@reduced graphene oxide. *Inorganic Chemistry Frontiers* **2018**, *5* (11), 2885-2892, 10.1039/C8QI00727F. DOI: 10.1039/C8QI00727F.
(17) Kang, D. M.; Shin, J.-I.; Kim, J. B.; Lee, K.; Chung, J. H.; Yang, H.-W.; Kim, K.-N.; Han, Y. S. Detection of 8-oxoguanine and apurinic/apyrimidinic sites using a fluorophore-labeled probe with cell-penetrating ability. *BMC Molecular and Cell Biology* **2019**, *20* (1), 54. DOI: 10.1186/s12860-019-0236-x.
(18) Chiorcea-Paquim, A.-M. 8-oxoguanine and 8-oxodeoxyguanosine Biomarkers of Oxidative DNA Damage: A Review on HPLC–ECD Determination. *Molecules* **2022**, *27* (5), 1620.
(19) Bochman, M. L.; Paeschke, K.; Zakian, V. A. DNA secondary structures: stability and function of G-quadruplex structures. *Nature Reviews Genetics* **2012**, *13* (11), 770-780. DOI: 10.1038/nrg3296.
(20) Burge, S.; Parkinson, G. N.; Hazel, P.; Todd, A. K.; Neidle, S. Quadruplex DNA: sequence, topology and structure. *Nucleic Acids Res.* **2006**, *34* (19), 5402-5415. DOI: 10.1093/nar/gkl655 From NLM.
(21) Miclot, T.; Corbier, C.; Terenzi, A.; Hognon, C.; Grandemange, S.; Barone, G.; Monari, A. Forever Young: Structural Stability of Telomeric Guanine Quadruplexes in the Presence of Oxidative DNA Lesions**. *Chem. Eur. J.* **2021**, *27* (34), 8865-8874, https://doi.org/10.1002/chem.202100993. DOI: https://doi.org/10.1002/chem.202100993 (acccessed 2022/01/24).
(22) Bielskutė, S.; Plavec, J.; Podbevšek, P. Oxidative lesions modulate G-quadruplex stability and structure in the human BCL2 promoter. *Nucleic Acids Res.* **2021**, *49* (4), 2346-2356. DOI: 10.1093/nar/gkab057 (acccessed 11/5/2021).
(23) Singh, A.; Kukreti, R.; Saso, L.; Kukreti, S. Oxidative Stress: Role and Response of Short Guanine Tracts at Genomic Locations. *Int. J. Mol. Sci.* **2019**, *20* (17), 4258.
(24) Bielskutė, S.; Plavec, J.; Podbevšek, P. Impact of Oxidative Lesions on the Human Telomeric G-Quadruplex. *J. Am. Chem. Soc.* **2019**, *141* (6), 2594-2603. DOI: 10.1021/jacs.8b12748.
(25) Friedman, A. E.; Chambron, J. C.; Sauvage, J. P.; Turro, N. J.; Barton, J. K. A molecular light switch for DNA: Ru(bpy)2(dppz)2+. *J. Am. Chem. Soc.* **1990**, *112* (12), 4960-4962. DOI: 10.1021/ja00168a052.
(26) Smith, J. A.; Collins, J. G.; Keene, F. R. Groove-Binding Ruthenium(II) Complexes as Probes of DNA Recognition. In *Metal Complex–DNA Interactions*, John Wiley & Sons, Ltd, 2009; pp 317-346.
(27) McConnell, A. J.; Lim, M. H.; Olmon, E. D.; Song, H.; Dervan, E. E.; Barton, J. K. Luminescent Properties of Ruthenium(II) Complexes with Sterically Expansive Ligands Bound to DNA Defects. *Inorganic Chemistry* **2012**, *51* (22), 12511-12520. DOI: 10.1021/ic3019524.
(28) Wachter, E.; Moyá, D.; Parkin, S.; Glazer, E. C. Ruthenium Complex “Light Switches” that are Selective for Different G-Quadruplex Structures. *Chem. Eur. J.* **2016**, *22* (2), 550-559. DOI: 10.1002/chem.201503203.
(29) Piraux, G.; Bar, L.; Abraham, M.; Lavergne, T.; Jamet, H.; Dejeu, J.; Marcélis, L.; Defrancq, E.; Elias, B. New Ruthenium-Based Probes for Selective G-Quadruplex Targeting. *Chem. Eur. J.* **2017**, *23*, 11872-11880. DOI: 10.1002/chem.201702076.
(30) Boynton, A. N.; Marcélis, L.; McConnell, A. J.; Barton, J. K. A Ruthenium(II) Complex as a Luminescent Probe for DNA Mismatches and Abasic Sites. *Inorganic Chemistry* **2017**, *56* (14), 8381-8389. DOI: 10.1021/acs.inorgchem.7b01037.
(31) Gill, M. R.; Thomas, J. A. Ruthenium(ii) polypyridyl complexes and DNA-from structural probes to cellular imaging and therapeutics. *Chem. Soc. Rev.* **2012**, *41* (8), 3179-3192, 10.1039/C2CS15299A. DOI: 10.1039/C2CS15299A.
(32) Deraedt, Q.; Marcelis, L.; Loiseau, F.; Elias, B. Towards mismatched DNA photoprobes and photoreagents: "elbow-shaped" Ru(ii) complexes. *Inorg. Chem. Front.* **2017**, *4* (1), 91-103, 10.1039/C6QI00223D. DOI: 10.1039/C6QI00223D.
(33) Gill, M. R.; Garcia-Lara, J.; Foster, S. J.; Smythe, C.; Battaglia, G.; Thomas, J. A. A ruthenium(II) polypyridyl complex for direct imaging of DNA structure in living cells. *Nat. Chem.* **2009**, *1* (8), 662-667. DOI: 10.1038/nchem.406 From NLM.
(34) Berrones Reyes, J.; Kuimova, M. K.; Vilar, R. Metal complexes as optical probes for DNA sensing and imaging. *Curr. Opin. Chem. Biol.* **2021**, *61*, 179-190. DOI: https://doi.org/10.1016/j.cbpa.2021.02.007.
(35) Jiang, J.; Teunens, T.; Tisaun, J.; Denuit, L.; Moucheron, C. Ruthenium(II) Polypyridyl Complexes and Their Use as Probes and Photoreactive Agents for G-quadruplexes Labelling. *Molecules* **2022**, *27* (5), 1541.
(36) Gillard, M.; Piraux, G.; Daenen, M.; Abraham, M.; Troian-Gautier, L.; Bar, L.; Bonnet, H.; Loiseau, F.; Jamet, H.; Dejeu, J.; et al. Photo-oxidizing Ruthenium(II) Complexes with Enhanced Visible Light Absorption and G-quadruplex DNA Binding Abilities. *Chem. Eur. J.* **2022**, *n/a* (n/a). DOI: https://doi.org/10.1002/chem.202202251.
(37) Weynand, J.; Episkopou, H.; Le Berre, G.; Gillard, M.; Dejeu, J.; Decottignies, A.; Defrancq, E.; Elias, B. Photo-induced telomeric DNA damage in human cancer cells. *RSC Chemical Biology* **2022**, 10.1039/D2CB00192F. DOI: 10.1039/D2CB00192F.
(38) Weynand, J.; Diman, A.; Abraham, M.; Marcélis, L.; Jamet, H.; Decottignies, A.; Dejeu, J.; Defrancq, E.; Elias, B. Towards the Development of Photo-Reactive Ruthenium(II) Complexes Targeting Telomeric G-Quadruplex DNA. *Chem. Eur. J.* **2018**, *24* (72), 19216-19227. DOI: doi:10.1002/chem.201804771.
(39) Gillard, M.; Weynand, J.; Bonnet, H.; Loiseau, F.; Decottignies, A.; Dejeu, J.; Defrancq, E.; Elias, B. Flexible RuII Schiff Base Complexes: G-Quadruplex DNA Binding and Photo-Induced Cancer Cell Death. *Chem. Eur. J.* **2020**, *26* (61), 13849-13860, https://doi.org/10.1002/chem.202001409. DOI: https://doi.org/10.1002/chem.202001409 (acccessed 2021/02/08).
(40) Gillard, M.; Laramée-Milette, B.; Deraedt, Q.; Hanan, G. S.; Loiseau, F.; Dejeu, J.; Defrancq, E.; Elias, B.; Marcélis, L. Photodetection of DNA mismatches by dissymmetric Ru(ii) acridine based complexes. *Inorg. Chem. Front.* **2019**, *6* (9), 2260-2270. DOI: 10.1039/C9QI00133F.
(41) Amouyal, E.; Homsi, A.; Chambron, J.-C.; Sauvage, J.-P. Synthesis and study of a mixed-ligand ruthenium(II) complex in its ground and excited states: bis(2,2[prime or minute]-bipyridine)(dipyrido[3,2-a : 2[prime or minute],3[prime or minute]-c]phenazine-N4N5)ruthenium(II). *Journal of the Chemical Society, Dalton Transactions* **1990**, (6), 1841-1845, Article Journal.
(42) Deraedt, Q.; Marcélis, L.; Auvray, T.; Hanan, G. S.; Loiseau, F.; Elias, B. Design and Photophysical Studies of Acridine-Based RuII Complexes for Applications as DNA Photoprobes. *Eur. J. Inorg. Chem.* **2016**, *2016* (22), 3649-3658. DOI: 10.1002/ejic.201600468.
(43) Brouwer, A. M. Standards for photoluminescence quantum yield measurements in solution (IUPAC Technical Report). *Pure and Applied Chemistry* **2011**, *83* (12), 2213-2228.
(44) McGhee, J. D.; von Hippel, P. H. Theoretical aspects of DNA-protein interactions - Cooperative and non-cooperative binding of large ligands to a one-dimensional homogeneous lattice. *J. Mol. Biol.* **1974**, *86*, 469-489. DOI: 10.1016/0022-2836(74)90031-x.
(45) Wallner, J.; Lhota, G.; Jeschek, D.; Mader, A.; Vorauer-Uhl, K. Application of Bio-Layer Interferometry for the analysis of protein/liposome interactions. *Journal of Pharmaceutical and Biomedical Analysis* **2013**, *72*, 150-154. DOI: https://doi.org/10.1016/j.jpba.2012.10.008.
(46) Picault, L.; Laigre, E.; Gillon, E.; Tiertant, C.; Renaudet, O.; Imberty, A.; Goyard, D.; Dejeu, J. Characterization of the interaction of multivalent glycosylated ligands with bacterial lectins by biolayer interferometry. *Glycobiology* **2022**, *32* (10), 886-896. DOI: 10.1093/glycob/cwac047 (acccessed 9/28/2022).

Table of Contents